Soft Matter

RSC Publishing

PAPER

View Article Online
View Journal | View Issue

Ethanol shock and lysozyme aggregation

Cite this: *Soft Matter*, 2013, **9**, 2187

Louis R. Nemzer,*[a] Bret N. Flanders,[b] Jeremy D. Schmit,[b] Amitabha Chakrabarti[b] and Christopher M. Sorensen[b]

Received 14th September 2012
Accepted 17th December 2012

DOI: 10.1039/c2sm27124a

www.rsc.org/softmatter

Irreversible protein–protein aggregation is associated with several human maladies, including Alzheimer's disease, and poses a challenge to pharmaceutical formulation and preservation efforts. The existence of multiple agglomeration pathways that lead to different final morphologies complicates the ability to determine the aggregation fate of proteins under various reaction conditions. Using lysozyme (3 mg mL^{-1}) as a model protein for dynamic light scattering and circular dichroism studies, we observed dense, non-fibrous aggregation triggered under acidic (pH 4) conditions by a destabilizing "ethanol shock" of 16% (v/v) ethanol. However, ethanol concentrations 15% and below did not lead to aggregation. The aggregation fate of these proteins is thus found to be extremely sensitive to the denaturant concentration. We introduce a stochastic model to explain this dependence based on the denaturant-induced population of a partially unfolded state.

Introduction

Protein aggregation possesses a rich phase-diagram replete with interesting physics. The process also has important practical applications throughout the biomedical industry. The abnormal aggregation of misfolded[1,2] proteins into insoluble fibril-like structures known as amyloids has been associated with several neurodegenerative disorders.[3] Amyloid aggregates have been observed in proteins not related to human disease, including lysozyme, the protein that is the subject of this work. Hill *et al.*[4,5] have shown that amyloid fibrils can be obtained by destabilizing a solution of chicken egg white lysozyme *via* incubation at 50 °C. However, quasi-1D amyloid fibrils are only one of several possible final morphologies accessible to aggregating proteins. A dense agglomeration can also be formed *via* kinetics that reflect its three-dimensional isotropy. This pathway is of particular concern to the pharmaceutical industry,[6] in which biotic doses can be rendered unusable by the agglomeration of constituent proteins.[7] Therefore, understanding the conditions that give rise to aggregates, as well as the kinetics of that aggregation, is of particular importance.

The ability of proteins to aggregate at all depends on a partial unfolding[8,9] that disrupts tertiary structure but leaves key secondary motifs, especially beta-sheets,[10] intact. The general stability of the native-fold conformation under physiological conditions is thus an important inhibitor of possibly pathogenic aggregation in living systems. The behavior of proteins far from native conditions, for example, due to very low pH[11] or elevated temperatures, allows the study of stochastic processes with characteristic times too long to watch under physiological conditions. Thus, events that happen over the course of many years in natural environments may now occur rapidly enough for close, repeated observation. It has been proposed that at least some human protein aggregation conditions should be thought of as "stochastic" diseases, in light of the fact that onset may be rapid or delayed by many decades. This provides a strong motivation to study systems on the edge of metastability,[12] where small changes in reaction conditions may lead to very different qualitative outcomes. For example, gelation can be distinguished from nucleated aggregation by the complete lack of a lag phase, as borne out by computer simulations.[13] From a material fabrication point of view, homopolymer aggregation[14,15] from a binary mixture containing a poor solvent has already been shown to be very sensitive to the reaction conditions. Irreversible aggregation in general is usually seen as an undesirable process to be carefully avoided, as in pharmaceutical formulation and preservation, but may also be a vital aspect of fabrication methods, as in directed material self-assembly.[16]

We have used lysozyme from chicken egg white as a model system.[17,18] Using acidic conditions and low concentrations of ethanol to destabilize[19] the protein, we observed that the formation of aggregates is extremely sensitive to the ethanol concentration. Our experiments follow those conducted by Mushol and coworkers,[4] who found that lysozyme formed amyloid fibrils at low pH and elevated temperatures. However, our aggregates are consistent with dense spherical clusters, rather than fibrils, suggesting that elevated temperature and denaturants like ethanol have very different effects on the aggregation propensity of proteins.

[a]*Farquhar College of Arts and Sciences, Nova Southeastern University, Davie, FL 33314, USA. E-mail: Lnemzer@nova.edu*

[b]*Department of Physics, Kansas State University, Manhattan, KS 66506, USA*

Theory

Dynamic light scattering[20] (DLS) is a powerful,[21] nondestructive method for obtaining the size distribution of nano- and microscale particles.[22] The autocorrelation of scattered light intensity as a function to time, $g^{(2)}(\tau)$, captures the Brownian motion[23] of the particles and decays exponentially with a characteristic time that depends on[24] the hydrodynamic radius, R_H.[25] Since the scattering intensity from a single spherical particle much smaller than the wavelength of light varies as the square of its volume, the total intensity is expected to scale as $N(R_H)R_H$, [6]where N is the number of particles of that size. As a result, the scattered intensity increases markedly when monomers aggregate into oligomers. This effect makes light scattering especially well-suited to detect the onset of aggregation.

Experimental

Lysozyme (MP Biomedicals) was used without further purification. The protein was dissolved in either a phosphate (pH 2) or acetate (pH 4) buffer, sonicated for 60 min and then centrifuged at 14 000 RPM for 30 min. The supernatant was then passed through a syringe filter (0.2 μm) and diluted to a final (nominal) concentration of 3 mg mL^{-1}. Dynamic light scattering was performed using a home-built system, in which a 488 nm laser beam (Uniphase 2101-20SLE) was passed through a $\lambda/2$ waveplate to insure a vertical polarization before being focused with a lens on the sample volume. At time $t = 0$, an "ethanol shock" was initiated by adding a specific amount of ethanol, here expressed as a percentage (v/v) or mole fraction. The scattered light was collected with a second lens and passed through an adjustable vertical slit to a photomultiplier tube. An ALV5000 system recorded the autocorrelation function, which was analyzed using a cumulant[26] (semilog) fit, along with the DynaLS software package for Laplace inversion. The viscosity parameter was obtained by using an interpolating function based on the temperature and ethanol concentration.

All circular dichroism (CD) spectra were taken at pH 4 in the far-UV spectral region, with the protein diluted 30× compared to the DLS experiments (0.1 mg mL^{-1} *vs.* 3 mg mL^{-1}). This lysozyme concentration was too dilute for aggregation to occur, so the experiment captured the changes in the secondary structure of isolated proteins. To achieve this, 15 μL of the stock 3 mg mL^{-1} lysozyme solution was mixed with additional phosphate buffer, along with a calculated amount of ethanol, to achieve the desired denaturant concentration and a total final volume of 300 μL. The results of 5 scans were averaged and agreed well with literature spectra.

Results

Fig. 1 depicts the normalized intensity correlation functions $g^{(2)}(\tau)$ plotted against the natural logarithm of the lag time τ for a standard pH 2 lysozyme solution. The circles represent the protein monomers prior to ethanol shock. The filled squares denote the solution after the addition of 4% ethanol. The filled diamonds show the standard solution with 4% ethanol and 70 mM KCl. The solid lines are theoretical fits to these profiles that were obtained using the cumulant method.[27] This fitting procedure extracts unique determinations of the average hydrodynamic radius R_H of the scatterers in these solutions. In the standard solution, lysozyme was found to have a hydrodynamic radius of 2.2 nm, which is comparable to but slightly larger than previously reported values[28] for monomeric lysozyme, 2.1 nm, at pH 7. The addition of ethanol doubled the size to 4.5 nm. The subsequent addition of salt, 70 mM KCl, reduced the size back to 2.4 nm (Fig. 1). When these solutions were examined again after two weeks, we found no evidence of lysozyme aggregation, implying that aggregation does not readily occur at pH 2.

For pH 4, a first-pass experiment was done to find the concentration of ethanol required to induce aggregation. Ethanol concentrations above 28% led to rapid aggregation. After 4–6 hours, all of these samples exhibited clusters with maximum sizes near 1 micron, whereas only a doubling of size, but no aggregation, was observed below 15%. To gain insight into the aggregation mechanism, we focused on the transition region of ethanol concentrations. A closer look at a 15% sample at pH 4 shows that after 2 hours, the size had nearly doubled. Even after two weeks, however, no aggregation was observed. Fig. 2 depicts the natural log of $g^{(2)}(\tau)$ plotted against the lag time τ for lysozyme solutions at pH 4 consisting of the unperturbed solution (filled squares) and the solution following a 15% ethanol shock (filled circles). The hydrodynamic radius of the lysozyme monomers was 1.9 nm in the native solution, but increased to 3.6 nm in the shocked solution. For comparison, $g^{(2)}(\tau)$ for the calibration standard composed of 12.2 nm polystyrene spheres are shown (unfilled circles). The extracted R_H-values from these profiles indicate that the average lysozyme hydrodynamic radius increased by a factor of 1.9.

The addition of 16% ethanol induces more complex behavior. In marked contrast to both the high and low ethanol regimes, the addition of 16% ethanol produced a system that aggregated, but only after a lag time of varying lengths. Fig. 3 shows the total scattering intensity, divided by the initial intensity, overlaid with the extracted hydrodynamic radii from DLS. Scans were taken every minute and the correlation function from each was fitted to a double exponential decay. At early times, only a monomer signal can be discerned, shown as diamonds on the figure. After roughly 1 hour, a second decay signal, representing small aggregates (>50 nm, triangles), became evident. The mean hydrodynamic radius of these clusters grew until their signal overwhelmed the scattering from the monomers. This process was accompanied by a hundredfold increase in the total scattering intensity (line).

Fig. 4 shows the scattering intensity from five replicates at 16% ethanol at pH 4. Each trace was divided by its initial value before the ethanol shock. The profiles are well-fit by the sigmoidal function:

$$I(t) = 1 + \frac{I_f - 1}{1 + e^{-w(t - t_{mid})}} \quad (1)$$

in which $I(t)$ is the scattering intensity, I_f is the final intensity, w is the sigmoid width, and t_{mid} is the midpoint. While there

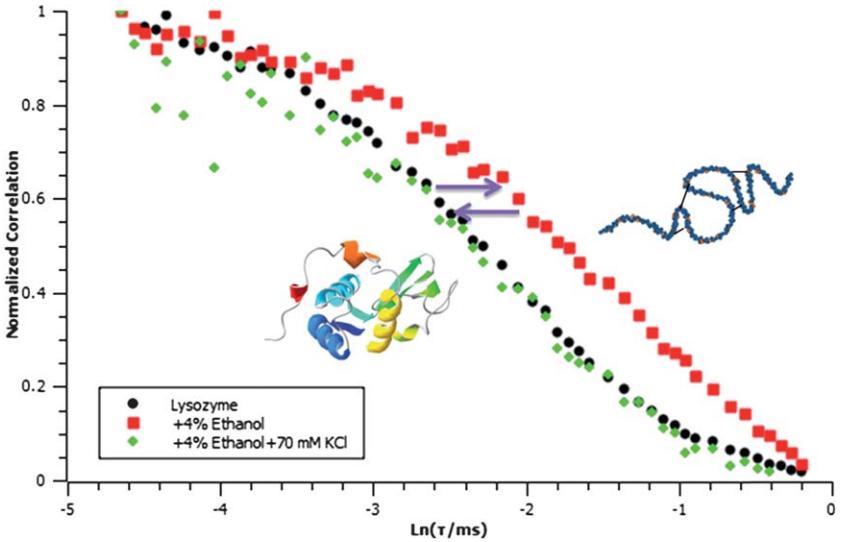

Fig. 1 Dynamic light scattering correlation traces for lysozyme at pH 2. The addition of ethanol shifted the correlation function to longer times, indicating a swelling of the polymer and a corresponding increase in hydrodynamic radius. The subsequent addition of a screening salt returned the size very close to its initial value. Overlaid is a cartoon representation of a partial unfolding of the native state, since complete denaturation, even under very adverse conditions, is prevented by the disulfide bridges (see Discussion section).

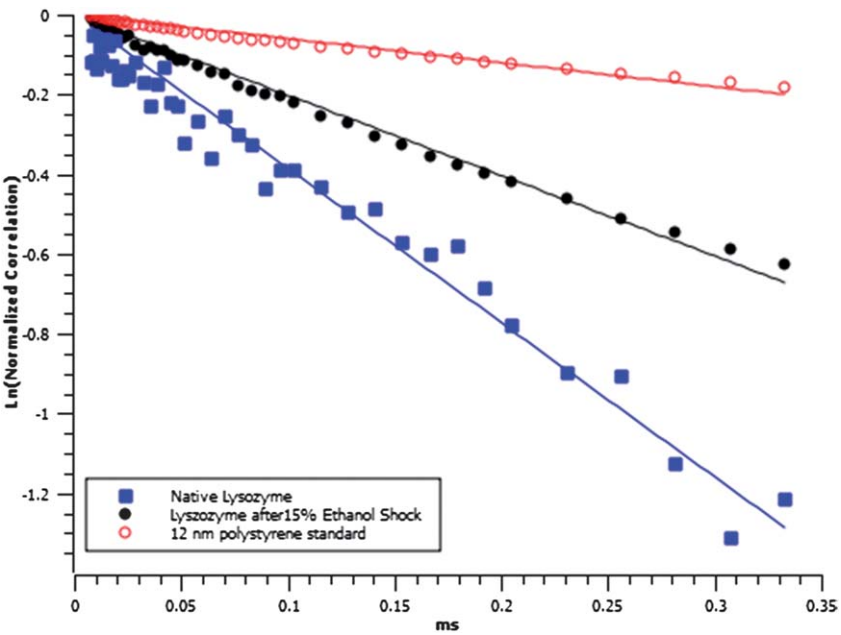

Fig. 2 15% ethanol at pH 4, using the cumulant fit representation. PS24 is a polystyrene standard of monodisperse 12 nm radius particles. The proteins experienced an increase in size by a factor of 1.9, from 1.9 nm to 3.6 nm.

are many ways to define the lag time, we choose the t_{mid} for this purpose, as this leads to minimal ambiguity. The stochastic nature of the process is apparent – the time to reach the midpoint of the sigmoidal fitting functions is random.

Fig. 5 plots R_H *versus* time for a lysozyme solution at pH 4 following a 17% ethanol shock. The data are well-fit by the function $at^{1/D}$, where a value of $1/D = 0.35$ was extracted from a non-linear least-squares method. In this case D, the effective fractal dimension,[29] is consistent with a dimensionality of 3, that is, a compact, dense spheroid. It is apparent that aggregation is much more rapid than observed following a 16% ethanol shock. Furthermore, the lag phase is barely discernible, and aggregates of radius 100 nm or more are present almost instantaneously.

To obtain a greater understanding of the folding conformations of the individual proteins at the various ethanol concentrations, we turned to circular dichroism spectroscopy.

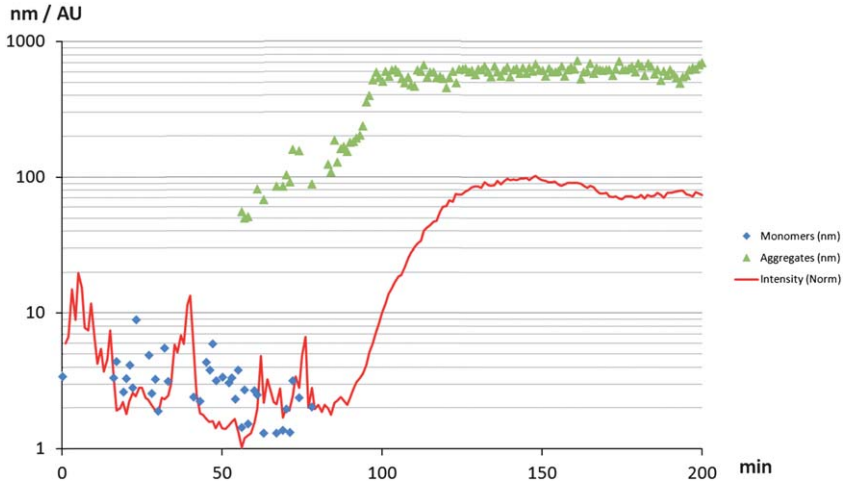

Fig. 3 Lysozyme hydrodynamic radius (diamonds and triangles, in nm) and normalized scattering intensity (line, AU) for an ethanol shock of 16%. At first, only monomers are observed, represented by the blue diamonds. After a lag time, small aggregates appear (green triangles), and eventually overwhelm the monomer signal. The onset of nucleation is accompanied by a large (hundred-fold) increase in the scattering intensity.

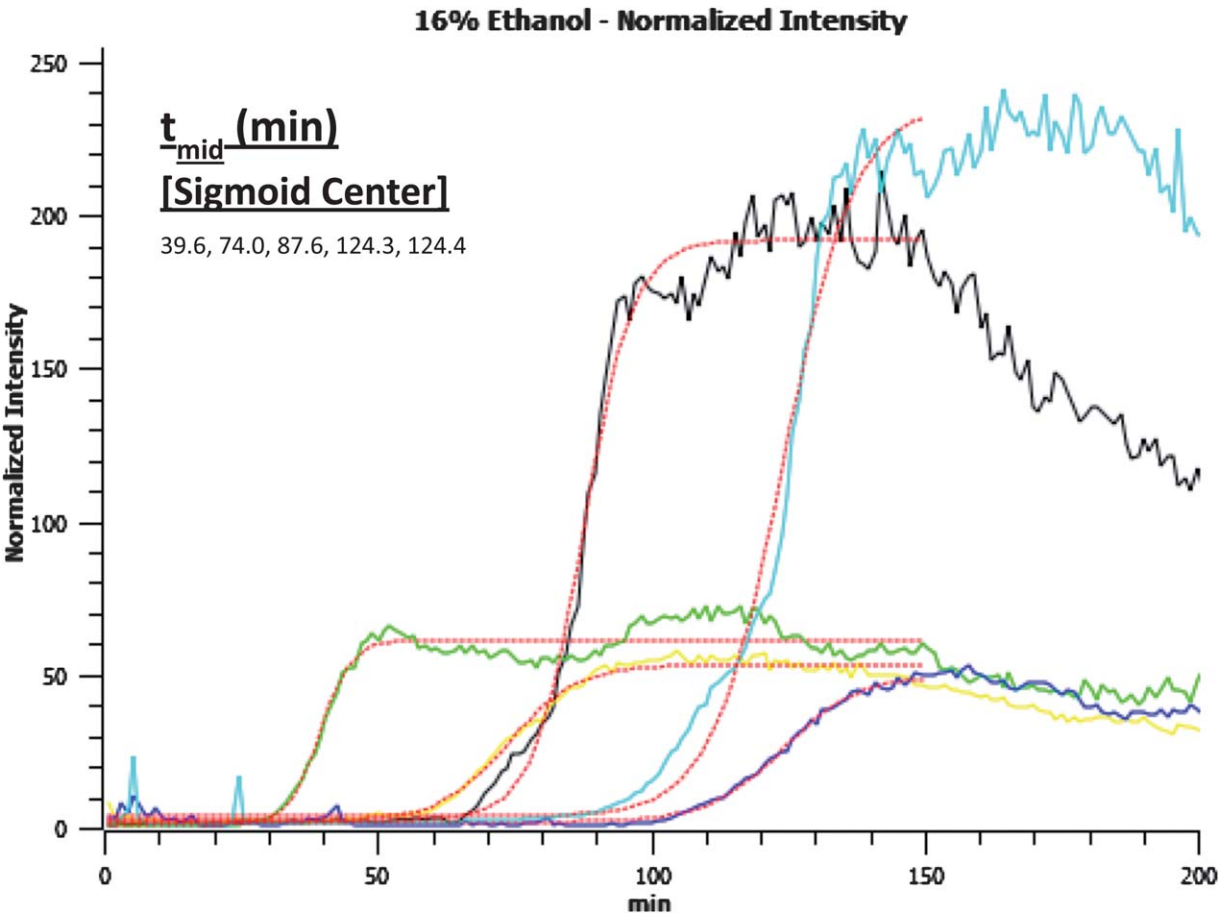

Fig. 4 Normalized intensity of five separate runs, with sigmoidal fits. The ethanol shock of 16% occurred for each at $t = 0$. The time each trace achieved its midpoint is also recorded.

For the CD protocol used, the largest possible ethanol concentration achievable was 97%, corresponding to no additional buffer being added. Fig. 6 depicts circular dichroism spectra for lysozyme solutions at pH 4 containing no ethanol (black line) and containing 97% ethanol (red line). The black profile agrees well with the spectrum for native lysozyme at neutral pH (dashed line) reported[30] in the literature. The spectrum changed very little as a result of the acidic

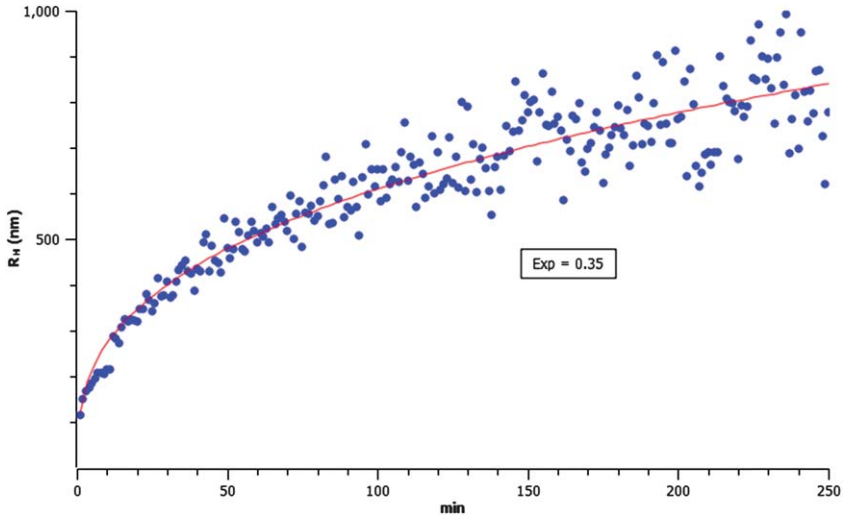

Fig. 5 17% ethanol shock. After an initial jump to about 100 nm, the hydrodynamic radius grows according to a power law, $R_H \sim t^{1/3}$, consistent with dense, compact spherical aggregation. This should be contrasted with the dimensionality of a fibril ($D = 1$) or fractal created by diffusion limited aggregation ($1 > D > 2$).

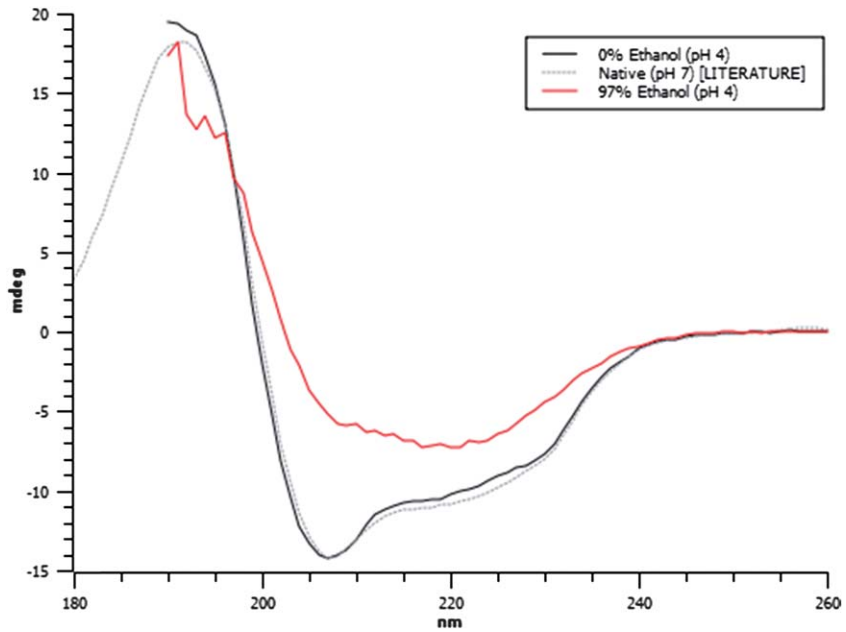

Fig. 6 CD spectra for native lysozyme at pH 4, literature spectra[30] at neutral pH, and lysozyme at pH 4 in 97% ethanol. Note the isodichroic point near 197 nm.

conditions, and, in fact, retained its basic features even in what was essentially pure ethanol. The spectral fits to alpha, beta, and random coil standard spectra (not shown), indicated that the primary change from the native state to the "denatured" state was a small loss of alpha helix. The isodichroic point, at which the samples display the same value of ellipticity, is found near 197 nm. This indicates a two-state transition, since the presence of multiple conformations would, in general, destroy this intersection. This is consistent with a native to partially unfolded transition as the primary driver of changes to the CD signal.

Fig. 7a shows the effect of intermediate ethanol concentrations on lysozyme in the range of 0–15%. The biggest change was observed to occur between no ethanol at all and the 2% ethanol sample. The CD signal jumps to more negative values at first, and then slowly changes back as the ethanol concentration was increased to 15%. Fig. 7b displays the traces from 15%, 16%, and 17% samples. These show a trend towards more negative ellipticities. Throughout all these graphs, however, the isodichroic point remains and signals from the secondary structure of the protein monomers stay intact.

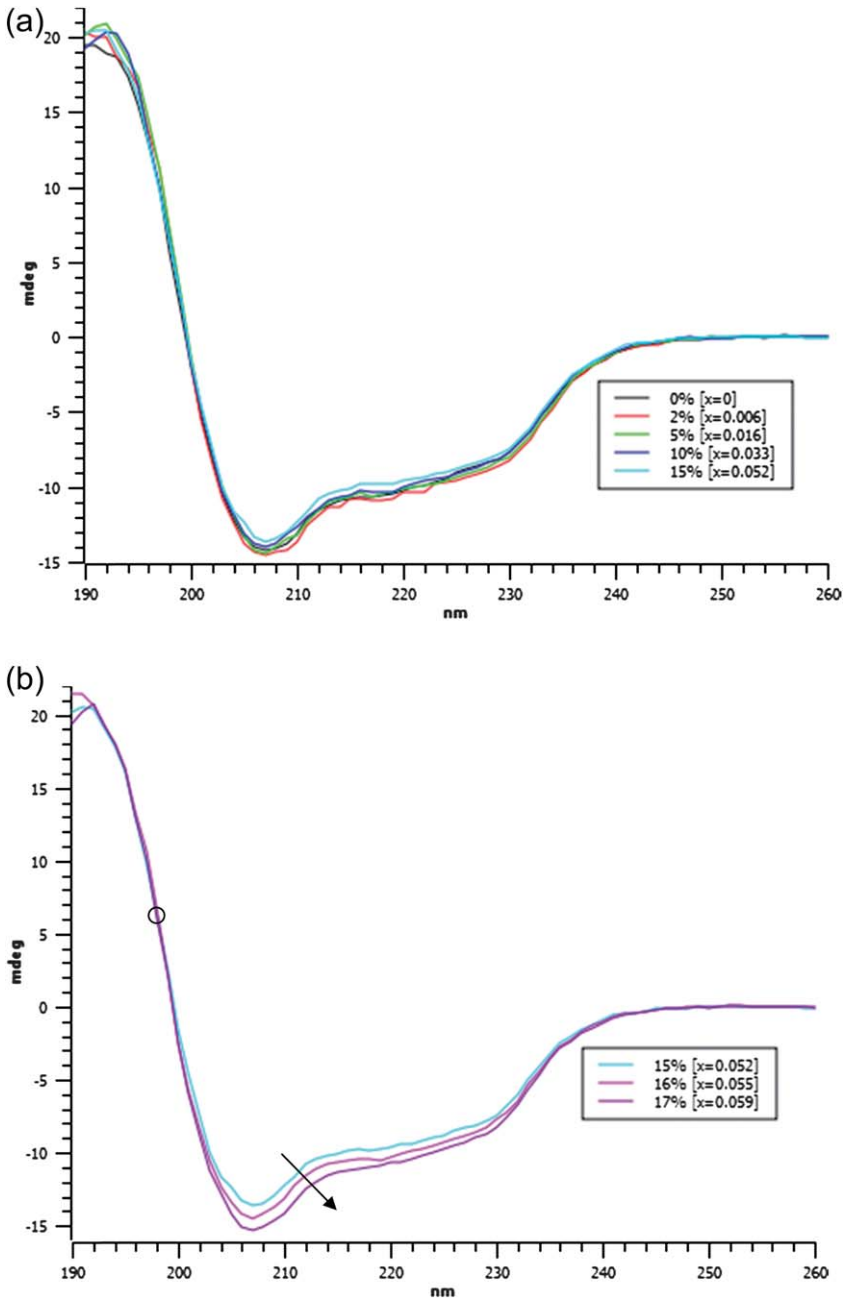

Fig. 7 (a) CD spectra between 0% and 15%. The largest jump occurs at very small (2%) ethanol concentrations. After that, there is a monotonic change until 15%. The quantity in the bracket is the equivalent ethanol mole fraction. (b) CD spectra for 15–17% ethanol. In this regime, increasing ethanol leads to larger (more negative) ellipticity. However, the isodichroic point remains.

Discussion

Lysozyme possesses four disulfide bridges, which collectively prevent a complete unfolding of the protein even under very adverse conditions.[31] Only in the presence of a reducing agent, which can break these S–S bonds, can lysozyme adopt a random coil configuration. This was confirmed by the CD data, which showed a slight loss of alpha-helix character, but not complete denaturation, even at very high ethanol concentrations. At low pH, amino acid residues on the lysozyme proteins are much more likely to be protonated. The strong positive charge enhances the intramolecular Coulombic repulsion between adjacent protonated residues. Denaturants like ethanol, which weaken the hydrophobic interaction between the nonpolar core residues and the solvent, further push the protein towards a partially unfolded state due to entropic considerations. The combined effect will be observed as a swelling of the protein and an increase in the hydrodynamic radius by a factor of 1.9.[31] Although core residues will now be exposed in this loosely folded state, aggregation with nearby proteins is not assured. A nucleation barrier may exist if the net attraction between the proteins is weak. Once a stable nucleus has been formed,

however, the attachment of additional partially unfolded proteins occurs spontaneously, since the energy cost is compensated by the large number of bonds that can form between the newcomer and proteins already in the cluster.

This explains the low ethanol concentration needed to partially unfold the protein at pH 2, and also why it did not aggregate under those conditions. At pH 2, lysozyme has an effective charge near +16.[32] The strongly charged protein has a large driving force towards an expanded conformation that distances the protonated residues from each other. Without any additional ethanol, this leads to a slightly swelled state compared to neutral pH. A small amount of denaturant is sufficient to push the equilibrium size to about twice its native value. However, aggregation cannot occur because the Coulombic repulsion prevents the close approach of other proteins. The addition of salt, which can sometimes precipitate (salt-out) proteins by screening these charges, only serves to refold the proteins.

At pH 4, the intraprotein electrostatic repulsion is reduced, so more ethanol is required to initiate unfolding. However, once this occurs, the nucleation barrier is smaller, so protein–protein aggregation can occur if the partially unfolded state is sufficiently populated (Fig. 8).

Prior to proposing our mathematical framework, an alternative explanation, involving solution effects, merits discussion. It is well-known that, at a critical mole fraction, binary solutions of water and certain alcohols experience a marked discontinuity of slope in many observable parameters when plotted against concentration, such as the compressibility and enthalpy of mixing. For lysozyme, it has been found that the enthalpy and entropy of denaturation attain a maximum at an ethanol mole fraction of 0.06.[33] The prevailing explanation for this behavior is that, below this concentration, the ethanol molecules can be completely sequestered in quasi-stable clathrate-like water cages characterized by a persistent hydrogen bonding network. However, if the ethanol concentration is increased above this critical value, they begin to cluster and can strongly effect the solvation of hydrophobic groups of proteins that are also present in the same solution.[34] While the effect of clathrate-like water cages may play a role in this system, the model alone is not sufficient to explain to stochastic distribution of lag times observed in this experiment. These lag times to achieve the midpoint of the sigmoidal fit to the total scattering intensity for various ethanol concentrations are shown in Fig. 9.

Model

We introduce here a simple mathematical model to explain the very sensitive dependence of the aggregation lag time on ethanol concentration. This stochastic framework welds classic nucleation theory (CNT) with a linear approximation for the effect of denaturants on the protein free energy landscape. CNT assumes that the free energy associated with a cluster of radius r is:

$$\Delta G = \frac{4\pi r^3}{3v_0}\Delta\mu + 4\pi\gamma r^2 \quad (2)$$

where the first term represents the (favorable) bulk energy from the contacts between the monomers, each with volume v_0, and the second is a (unfavorable) surface energy term parameterized by the surface tension γ. Here, we take the chemical potential $\Delta\mu$ to be a function of the supersaturation S:

$$\Delta\mu = kT\ln S = kT\ln\frac{f}{f_c} \quad (3)$$

where f is the protein volume fraction and f_c is the solubility limit of the aggregate under consideration. When $f < f_c$, growth will never be spontaneous. When $f > f_c$, the bulk energy is favorable, but at small cluster size the surface tension term dominates, so a thermally activated stochastic process is required to surmount the free energy barrier. However, if a

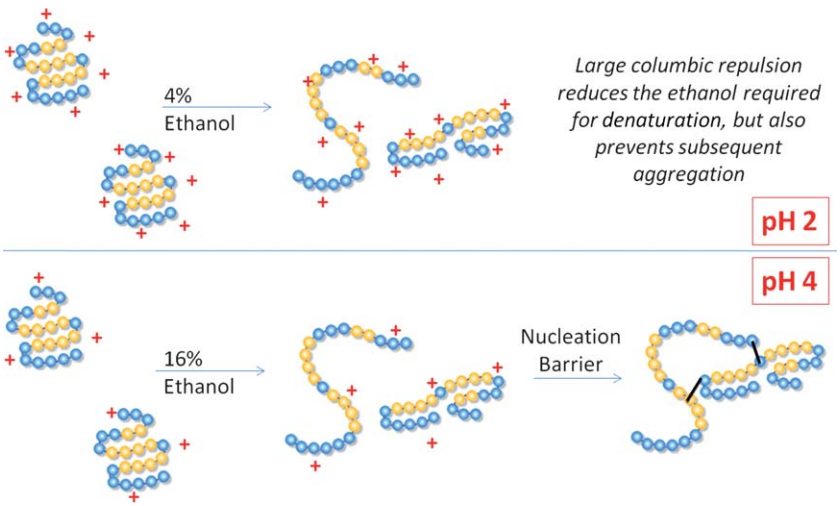

Fig. 8 Proposed aggregation model. The large positive charge on lysozyme at pH 2 creates a strong intraprotein repulsion that allows the protein to be partially unfolded by even a small amount of ethanol. However, the repulsion prevents subsequent protein–protein aggregation. In contrast, at pH 4, the protein undergoes partial unfolding at a higher ethanol concentration, but the nucleation barrier to aggregation is surmountable.

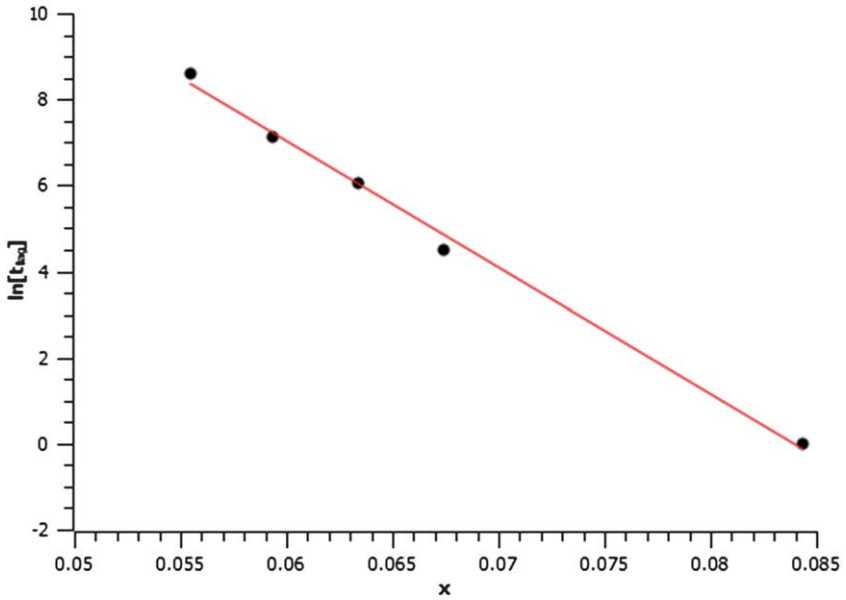

Fig. 9 Semilog fit of lag time in seconds *vs.* ethanol concentration, expressed as a mole fraction.

cluster can reach the critical nucleus size, $\frac{d(\Delta G)}{dr}$ changes sign, the addition of more monomers will be energetically favored. This critical size is $r^* = 2\gamma v_0/\Delta\mu$. The height of this nucleation barrier is then:

$$\Delta G^* = \Delta G(r = r^*) = \frac{16\pi {v_0}^2 \gamma^3}{3[kT \ln S]^2} \quad (4)$$

The rate of nucleation is expected to follow an Arrhenius form:

$$J = J_0 e^{-\Delta G^*/kT} \quad (5)$$

where J_0 is a possibly temperature dependent prefactor that relates to frequency of collisions between monomers in solution. CNT thus predicts a stochastic lag time for aggregation to occur. On a molecular level, this means the thermally activated random assembly of a nucleating cluster. The characteristic lag time for nucleation would then scale as:

$$t_{lag} \sim e^{B(\ln S)^{-2}} \quad (6)$$

where B is the dimensionless constant $\frac{16}{3}\pi {v_0}^2 \gamma^3/(kT)^3$.

Let us now assume that in our system only partially unfolded lysozyme monomers are "aggregation-competent,"[19] since the proteins that remain in their native conformation sequester their nonpolar residues within a hydrophobic core, and will not stick to other proteins. A linear approximation[35] of the effect of a denaturant concentration x on the free energy barrier between the native and partially unfolded states holds that:

$$\Delta G_{unfold} = \Delta G_0 + mx \quad (7)$$

where ΔG_0 is the free energy barrier in the absence of denaturant and $m < 0$ is an empirical parameter. The population of the unfolded state will therefore be:

$$f \sim e^{-\Delta G_{unfold}/kT} \sim f_{x=0} e^{-mx/kT} \quad (8)$$

here, $f_{x=0} = e^{-\Delta G_0/kT}$ is the unfolded population before the addition of denaturant. As a result, the natural log of the supersaturation, considering only the partially unfolded proteins, will be

$$\ln S = \ln \frac{f}{f_c} = \ln[f_{x=0}/f_c] - \frac{mx}{kT} \quad (9)$$

so

$$t_{lag} \sim e^{B\left[\ln\left(\frac{f_{x=0}}{f_c}\right) - \frac{mx}{kT}\right]^{-2}} \quad (10)$$

A slight reorganization of terms is instructive. Since, for the protein concentrations used in this experiment, the solution is clearly undersaturated by unfolded proteins in the absence of denaturant, $f_{x=0} < f_c$. Also, as alluded to previously, the effect of a denaturant is to stabilize the unfolded state relative to the native state, so m must be negative. We can then recast the quantity in the brackets as the difference of two non-negative terms:

$$t_{lag} \sim e^{B\left[\frac{|m|x}{kT} - \ln\left(\frac{f_c}{f_{x=0}}\right)\right]^{-2}} \quad (11)$$

The behavior of this expression is then more readily apparent. There is a critical value, $x^* = \frac{kT}{|m|}\ln\frac{f_{x=0}}{f_c}$, that represents the minimum denaturant concentration required to produce a saturated solution of unfolded monomers. As x increases from x^* to 1, the lag time is exponentially suppressed. Note that, based our assumptions about metastability existing only in the superstaturated state, the expression for t_{lag} is only valid for x larger than this asymptote, and spurious lag times at

lower denaturant concentrations should be ignored. In particular, t_{lag} diverges to infinity as the denaturant concentration approaches x^* from the right. Conversely, as x becomes large, the lag time rapidly approaches zero. This represents aggregation that occurs rapidly enough to be essentially instantaneous. For only a narrow window of denaturant concentrations will the lag time be distinctly observable on laboratory timescales. We justify the selection of a two-state model based on the CD spectra that showed a clear isodichroic point, as well the highly cooperative nature of protein folding.

Conclusions

Dynamic light scattering and circular dichroism were used to monitor the ethanol-induced aggregation of lysozyme under acidic conditions. We find that partial unfolding is a necessary,[36] but not sufficient, condition for aggregation. In lysozyme, complete denaturation is prevented by its four intramolecular disulfide bonds, but the partially unfolded state may still participate in irreversible protein–protein interactions. In this case, the aggregation fate is strongly dependent on the concentration of ethanol. Above a critical value, aggregation is stochastic process with a lag time that rapidly goes to zero at high concentrations. Below the critical concentration, aggregates are thermodynamically unfavorable and therefore absent. Although lysozyme is amyloidogenic, fibrils were never observed in this series of experiments. This is in contrast to the previous findings at elevated temperature, in which lysozyme formed amyloid fibrils,[4] confirming that fibrillation is only one possible aggregation pathway of biomedical import. Dense aggregation is of particular interest to pharmaceutical preparations on the edge of saturation. The expected spoilage over time will be depend on the degree of destabilization in a nonlinear fashion, since this form of aggregation requires a stochastic nucleating event in order to occur. This knowledge may be of particular interest in developing countries[37] where optimal storage conditions are not readily available.

Acknowledgements

The authors would like to express their deep appreciation to Robert Szoszkiewicz, Reggie Rice, John Tomich, Yasuaki Hiromasa, and Prem Thalpa for their assistance with this project.

References

1 S. Kumar, V. K. Ravi and R. Swaminathan, Suppression of lysozyme aggregation at alkaline pH by tri-*N*-acetylchitotriose, *Biochim. Biophys. Acta*, 2009, **1794**(6), 913–920.
2 D. J. Selkoe, Folding proteins in fatal ways, *Nature*, 2003, **426**, 900.
3 M. Xu, *et al.*, The first step of hen egg white lysozyme fibrillation, irreversible partial unfolding, is a two-state transition, *Protein Sci.*, 2007, **16**, 815–883.
4 S. E. Hill, J. Robinson, G. Matthews and M. Muschol, Amyloid protofibrils of lysozyme nucleate and grow *via* oligomer fusion, *Biophys. J.*, 2009, **96**, 3781–3790.
5 S. E. Hill, T. Miti, T. Richmond and M. Muschol, Spatial extent of charge repulsion regulates assembly pathways for lysozyme amyloid fibrils, *PLoS One*, 2011, **6**(4), e18171.
6 N. J. Agrawal, *et al.*, Aggregation in protein-based biotherapeutics: computational studies and tools to identify aggregation-prone regions, *J. Pharm. Sci.*, 2011, **100**, 5081–5095.
7 D. Shukla, C. P. Schneider and B. L. Trout, Molecular level insight into intra-solvent interaction effects on protein stability and aggregation, *Adv. Drug Delivery Rev.*, 2011, **63**, 1074–1085.
8 M. Dumoulin, *et al.*, A camelid antibody fragment inhibits the formation of amyloid fibrils by human lysozyme, *Nature*, 2003, **424**, 783.
9 A. Dhulesia, *et al.*, Local cooperativity in an amyloidogenic state of human lysozyme observed at atomic resolution, *J. Am. Chem. Soc.*, 2010, **132**(44), 15580.
10 P. T. Lansbury, *et al.*, Structural model for the amyloid fibril based on interstrand alignment of an antiparallel-sheet comprising a C-terminal peptide, *Nat. Struct. Biol.*, 1995, **2**, 990–998.
11 W. Dzwolak, *et al.*, Template-controlled conformational Patterns of insulin fibrillar self-assembly reflect history of solvation of the amyloid nuclei, *Phys. Chem. Chem. Phys.*, 2005, **7**, 1349–1351.
12 L. R. Nemzer and A. J. Epstein, Exciton peak redshifting and broadening in polyaniline chains during ion-induced hydrophobic collapse and aggregation, *Synth. Met.*, 2011, **161**, 2284–2288.
13 T. Perez, J. Gunton and A. Chakrabarti, Effects of the range and strength of interparticle attraction on gelation, *Bull. Am. Phys. Soc.*, 2011, 1121.
14 L. R. Nemzer, A. Schwartz and A. J. Epstein, Enzyme entrapment in reprecipitated polyaniline nano- and microparticles, *Macromolecules*, 2010, **43**, 4324–4330.
15 L. R. Nemzer and A. J. Epstein, A polyaniline-based optical biosensing platform using an entrapped oxidoreductase enzyme, *Sens. Actuators, B*, 2010, **150**, 376–383.
16 B. N. Flanders, Directed electrochemical nanowire assemby: precise nanostructure assembly *via* dendritic solidification, *Mod. Phys. Lett. B*, 2012, **26**(1), 1130001.
17 A. J. Trexler and M. R. Nilsson, The formation of amyloid fibrils from proteins in the lysozyme family, *Curr. Protein Pept. Sci.*, 2007, **8**(6), 537–557.
18 X. Chen, *et al.*, Universal isolation of cross-linked peptides: application to neurofibrillary tangles, *Bioconjugate Chem.*, 1999, **10**(1), 112.
19 S. Grudzielanek, R. Jansen and R. Winter, Solvational tuning of the unfolding, aggregation and amyloidogenesis of insulin, *J. Mol. Biol.*, 2005, **351**, 879–894.
20 U. Nobbmann, *et al.*, Dynamic light scattering as a relative tool for assessing the molecular integrity and stability of monoclonal antibodies, *Biotechnol. Genet. Eng. Rev.*, 2007, **24**, 117–128.
21 W. W. Wilson, Light scattering as a diagnostic for protein crystal growth—a practical approach, *J. Struct. Biol.*, 2003, **142**(1), 56–65.

22 V. Mikol, E. Hirsch and R. Giege, Monitoring protein crystallization by dynamic light scattering, *FEBS Lett.*, 1989, **258**(1), 63–66.
23 W. H. Gallagher and C. K. Woodward, The concentration dependence of the diffusion coefficient for bovine pancreatic trypsin inhibitor: a dynamic light scattering study of a small protein, *Biopolymers*, 1989, **28**(11), 2001–2024.
24 T. A. P. Seery, M. Angelopoulous, K. Levon and A. Seghal, Solution properties of polyaniline by light scattering measurements: achieving spatial homogeneity, *Synth. Met.*, 1997, **84**, 79–80.
25 B. Jachimska, M. Wasilewska and Z. Adamczyk, Characterization of globular protein solutions by dynamic light scattering, electrophoretic mobility, and viscosity measurements, *Langmuir*, 2008, **24**(13), 6866–6872.
26 D. E. Koppel, Analysis of macromolecular polydispersity in intensity correlation spectroscopy: the method of cumulants, *J. Chem. Phys.*, 1972, **57**(11), 4814–4820.
27 B. J. Frisken, Revisiting the method of cumulants for the analysis of dynamic light-scattering data, *Appl. Opt.*, 2001, **40**(24), 4087–4091.
28 W. Eberstein, Y. Georgalis and W. Saenger, Molecular interactions in crystallizing lysozyme solutions studied by photon correlation spectroscopy, *J. Cryst. Growth*, 1994, **143**(1–2), 71–78.
29 S. J. Khan, C. M. Sorensen and A. Chakrabarti, Kinetics and morphology of cluster growth in a model of short-range attractive colloids, *J. Chem. Phys.*, 2009, **131**, 194908.
30 J. G. Lees, *et al.*, A reference database for circular dichroism spectroscopy covering fold and secondary structure space, *Bioinformatics*, 2006, **22**(16), 1955–1962, http://pcddb.cryst.bbk.ac.uk/record.php?id=CD0000045000&dt=1.
31 I. K. Voets, *et al.*, DMSO-induced denaturation of hen egg white lsyozyme, *J. Phys. Chem. B*, 2010, **114**, 11875–11883.
32 S. A. Allison, M. Potter and J. A. McCammon, Modeling the electrophoresis of lysozyme, *Biophys. J.*, 1997, **73**, 133–140.
33 S. Cinelli, G. Onori and A. Santucci, Effect of aqueous alcohol solutions on the thermal transition of lysozyme: a calorimetric study, *J. Phys. Chem.*, 1997, **101**, 8029–8034.
34 V. Calandrini, G. Onori and A. Santucci, Examination by dynamic light scattering of lysozyme in water–alcohol mixtures, *J. Mol. Struct.*, 2001, **565–566**, 183–188.
35 S. T. Witten, *et al.*, The origin of pH-dependent changes in *m*-values for the denaturant-induced unfolding of proteins, *J. Mol. Biol.*, 2001, **309**, 1165–1175.
36 W. Dzwolak, *et al.*, Ethanol-perturbed amyloidogenic self-assembly of insulin: looking for origins of amyloid strains, *Biochemistry*, 2005, **44**, 8948–8958.
37 H. Thorsteinsdóttir, M. Ray, A. Kapoor and A. S. Daar, Health biotechnology innovation on a global stage, *Nat. Rev. Microbiol.*, 2011, **9**, 137–143.

